Asymmetric x-ray diffraction by strained crystal wafers: 8×8-matrix dynamical theory

D. W. Berreman and A. T. Macrander
AT&T Bell Laboratories, Murray Hill, New Jersey 07974
(Received 27 July 1987)

We have extended the matrix representation of the dynamical theory of x-ray diffraction to include Bragg planes that are oblique with respect to the surface of a crystal wafer. In place of the two independent 2×2 matrices of the Abelès method for planes parallel to the surface, we use a single 8×8 matrix. With such a matrix, rays may be skew with respect to the oblique Bragg planes and the wafer surface. Despite minor differences in approximations, computations by this method give results nearly identical to those from the Laue method in cases where either may be used. The new approach brings out the close analogy between the diffraction of visible light by blazed gratings and the diffraction of x rays by edges of oblique Bragg planes near the crystal surface. Matrix methods present no special problem in cases where the layers near the surface do not have the same spacing normal to the surface as those deeper down, resulting in curved oblique planes. Thus, epitaxial layers of varying composition, crystals strained by ion implantation, and other orderly surface distortions can be treated as easily as uniform wafers, as long as distorted three-dimensional order remains. Another advantage of matrix methods is that refraction and external and internal surface reflections are included in the computation automatically. An additional set of diffracting Bragg planes parallel to the surfaces can be included with little complication, thus allowing investigation of double-diffraction effects at the intersection of two diffraction cones.

I. INTRODUCTION

Most current descriptions of the dynamical theory of x-ray diffraction for perfect crystals in which the Bragg planes are not parallel to the surface are based on work culminated by von Laue in the 1930s.[1] The main emphasis is on the normal modes of propagation inside an ideal crystal, with the electromagnetic field outside matched to the normal modes. A different approximate analysis of diffraction by unstrained crystals with periodicity along the surface, in the limit of small grazing angles, was recently developed to help in the interpretation of grazing-incidence experimental data.[2] Dynamical theory for distorted crystals, based on the reciprocal-lattice point of view of von Laue, has been developed by Takagi[3] and Taupin.[4]

A different 8×8 matrix approach to dynamical theory, in which direct space rather than reciprocal space is in the forefront, will be described here. The method is particularly suited to numerical solution with a computer. The matrix method can be used to solve problems in ideal, undistorted crystals with high precision for any angle of incidence, including near-grazing incidence. In addition, the method is easy to apply to problems where periodicity of oblique Bragg planes varies in the direction normal to the surface because of strain induced, for example, by variation of composition with depth. The description of the distortion in direct space is easy to understand and to put into a data file.

We treat the crystal wafer as if it were composed of a stack of weakly diffracting gratings with equal grating spacing, g, and with parallel "rulings," but the other optical parameters of each grating in the stack need not be related. Each grating layer is parallel to the surface. One such layer, with various orders of diffraction, is illustrated in Fig. 1. If successive gratings are parallel and have equal spacing, but are displaced by a varying amount, we have our model of a strained ideal oblique-cut crystal, as shown in Fig. 2. Figure 3 is a projected three-dimensional illustration of a *blazed* grating showing coordinates out of the (xy) plane. The blazes may be thought

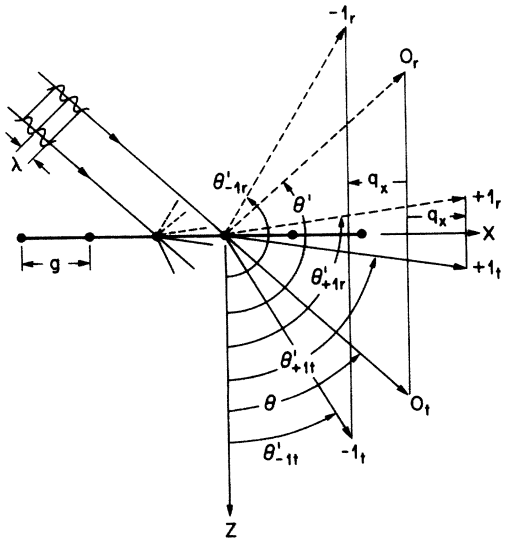

FIG. 1. Geometry of thin partially reflecting grating in the (xy) plane with reflection in the (xz) plane, showing coordinate system. Incident, ±first-order, and zeroth-order diffracted beams, both transmitted and reflected, are also shown. Azimuth ϕ and y axes are toward the reader and not shown. λ is the x-ray wavelength and g is the grating spacing.

 ©1988 The American Physical Society

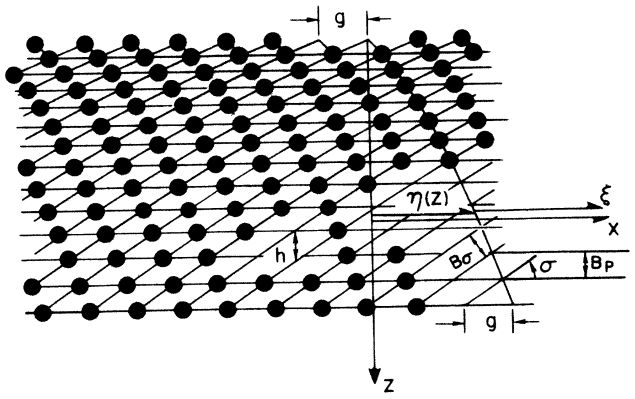

FIG. 2. Cross section of crystal wafer in relation to (xz) coordinate system in Fig. 1, showing curved Bragg planes and "blazed" surface. Varying tilt angle, σ, and Bragg spacings, B_σ and B_p, are also shown, together with gliding horizontal coordinate, ξ, and other variables. Strain-induced curvature of Bragg planes is exaggerated. Structure is assumed to be periodic or continuous in the y direction.

of as the edges of oblique Bragg-plane surfaces.

As a concrete example, consider a wafer of indium phosphide, which is a cubic crystal with sphalerite (diamond-like) structure having a unit-cell dimension $a=5.869\,28$ Å in its unstrained state. Consider a wafer cut parallel to the (111) planes. Let the y direction coincide with the edges of the emerging (200) planes, which slope at a tilt angle $\sigma=54.7356°$ with respect to the surface, as defined in Fig. 3. The Bragg spacing of the (200) planes is $B_\sigma=a/2=2.984\,64$ Å. The grating spacing along the x direction on the surface is $g=B_\sigma/\sin\sigma=3.594\,19$ Å. The crystal acts as a blazed grating for x rays with this grating spacing and with a diffraction envelope that is peaked toward the Bragg-reflection direction; the mirror direction for the tilted Bragg planes. For completeness, we mention here that the (111) planes have a Bragg spacing $B_p=a/\sqrt{3}=3.388\,63$ Å. Subsequent numerical results will be based on this example.

The 4×4 matrix method for treating *lamellar* structures[5,6,7] is exact. For *isotropic* lamellar structures the Abelès 2×2 matrix method is equivalent and also exact.[8] The 8×8 matrix method to be described is an extension of the 4×4 method, with dynamical perturbation by periodic *lateral* variations in the x direction. Any approximation errors in the method are attributable to the assumption that the *lateral* periodic variation of refractive index is much less than unity.

The 8×8 matrix approach to dynamical theory for unsymmetrical Bragg or Laue diffraction may also be regarded as a specialization and adaptation for x rays, of work by Rokushima and Yamakita[9] that was intended for visible-light optics. The 2×2 dynamical theory of symmetrical Bragg diffraction of x rays, based on the Abelès method,[10] might be thought of as a similar specialization of the exact 4×4 matrix optics for general lamellar anisotropic structures.

Although not restricted to dielectric properties that vary sinusoidally in the direction *normal* to the surfaces, the computation can be made very efficient when such periodicity exists, even over limited distances.

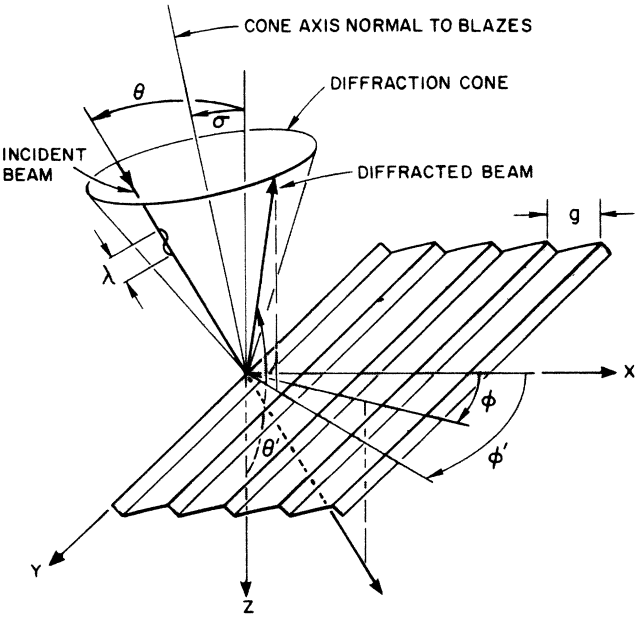

FIG. 3. Three-dimensional view of blazed grating showing negative first-order skew diffraction together with angles θ and ϕ, the (xyz) coordinate system, and the diffraction cone.

II. OPTICS OF A THIN PARTIALLY REFLECTING GRATING

Consider a thin partially reflecting sheet in the (xy) plane with periodic variation of optical properties in the x direction having a grating spacing g. If a source of radiation of wavelength λ is at a distant point above the sheet, then specular reflection by the sheet creates a virtual source at the same angle below the sheet. If the incident beam is in the (xz) plane and the angle between the z axis and the incident beam is θ, as shown in Fig. 1, then diffracted beams will occur at polar angles θ'_n above and below the plane given by the grating equation

$$n\lambda=g(\sin\theta'_n-\sin\theta)\,, \tag{1}$$

where n is the diffraction order $(0,\pm1,\pm2,\ldots)$. As a special case, if the dots on the grating shown in Fig. 1 are at the intersection of the x axis with crystalline Bragg planes in the (yz) plane, then Eq. (1), with $\theta'_n=-\theta$ and g equal to the Bragg spacing, is Bragg's law, $n\lambda=2g\sin\theta$, for nth-order symmetrical Laue (transmissive) diffraction.

We are interested in cases where the incident beam may be skew with respect to the (xz) plane. Let the grating lines be in the y direction, off the page in Figs. 1 and 2, and consider a polar-coordinate system wherein θ is measured from the z axis at any azimuth, and the azimuth ϕ is measured out from the x axis toward the $+y$ direction. The beams in Fig. 1 are then all at zero az-

imuth. A generalization of Eq. (1) is

$$nq_x = k(\sin\theta'_n\cos\phi'_n - \sin\theta\cos\phi) \equiv k'_{xn} - k_x \ , \tag{2}$$

where $q_x \equiv 2\pi/g$ is the "momentum" imparted to the diffracted beam by the grating, $k \equiv 2\pi/\lambda$ is the magnitude of the x-ray propagation vector, and k_x and k_y are components of the vector. This, together with the auxiliary equation

$$k_y \equiv k\sin\theta\sin\phi = k'_y \equiv k\sin\theta'\sin\phi' \ , \tag{3}$$

define the directions of the diffracted rays. Another way of looking at the latter two equations is to consider that nothing changes the y momentum, k_y, of the beam, but reflection can reverse the sign on k_z. At the same time, the grating can add momentum q_x to the beam and k_z is altered to preserve total momentum, k.

A little-known fact about diffraction gratings is that as a monochromatic source is moved in a circle about a fixed bisector of the angle between the incident beam and any diffracted beam, then the diffracted ray will always pass through the opposite point on the circle, as shown in Fig. 3. The cone formed in this process is the same as the better-known diffraction cone in the x-ray optics of crystals,[1] but ordinary gratings do not impose the Bragg restriction on the angle of incidence for diffraction of the monochromatic beam. A blazed grating diffracts light most efficiently near the direction of specular reflection of the blazes, which corresponds to the Bragg reflection direction for x-ray diffraction. In the limit of very broad shallow blazes, the band of appreciable diffraction becomes very narrow and the Bragg equation describes the center of the diffraction envelope. Similarly, when Bragg planes are tilted with respect to the surface of a crystal, they act as a diffraction grating for x rays. If the penetration of the beam is small because of high absorption or grazing incidence angle, only narrow edges of the Bragg planes influence the diffraction. Then the range of wavelengths or angles over which appreciable diffraction occurs may be much broader than the usual Darwin bandwidth or rocking-curve width. The spectral resolution of the grating in either x-ray diffraction or grating diffraction depends on the number of coherent grating lines, not on the narrowness of the Darwin or diffraction band.

III. VECTOR REPRESENTATION OF FIELDS

The electromagnetic field components in the (xy) plane, of a plane wave intersecting that plane at a particular angle, can be defined by $\Psi_0 e^{i(k_x x + k_y y - \omega t)}$, where Ψ_0 is the four-dimensional vector[7]

$$\Psi_0 = \begin{bmatrix} E_x \\ H_y \\ E_y \\ -H_x \end{bmatrix} , \tag{4}$$

where E and H are electric and magnetic field components.

We shall suppose that the (xy) plane is parallel to the two parallel surfaces of a crystal wafer, with gas or vacuum at the first surface and any homogeneous isotropic dielectric material at the other. We shall also suppose that one set of Bragg planes intersects the interfaces along lines parallel to the y direction and that, among the *oblique* planes, only one set is close to obeying the Bragg condition for the incident beam. However, the possibility that planes parallel to the surface may simultaneously diffract either the incident beam or the beam diffracted from the oblique planes will not be excluded. Thus, investigation of double-diffraction effects at the intersection of two diffraction cones,[1] an effect equivalent to the intersection of two Kossel lines except that the x rays originate outside the crystal, is possible. (A study of double diffraction with a second set of planes not parallel to the surface by matrix methods would require 12×12 matrices and would be considerably more complicated.)

Considering the crystal surface as a diffraction grating, it is easy to show that the diffracted beams of first order may be represented by the four-element diffracted wave vector $\Psi_d e^{i[(k_x+q_x)x + k_y y - \omega t]}$ where $q_x = \pm 2\pi/g$, and

$$\Psi_d = \begin{bmatrix} E_{xd} \\ H_{yd} \\ E_{yd} \\ -H_{xd} \end{bmatrix} . \tag{5}$$

It is convenient to begin the development of the 8×8 matrix method by defining the eight-element vector,

$$\Psi = \begin{bmatrix} E_x \\ H_y \\ E_y \\ -H_x \\ E_{xd}e^{iq_x x} \\ H_{yd}e^{iq_x x} \\ E_{yd}e^{iq_x x} \\ -H_{xd}e^{iq_x x} \end{bmatrix} . \tag{6}$$

All of the electromagnetic field components of appreciable amplitude on any plane parallel to the surface of the crystal are then defined by $\Psi e^{i(k_x x + k_y y - \omega t)}$.

IV. MAXWELL'S EQUATIONS

Two of Maxwell's equations in an isotropic dielectric medium may be written in Gaussian units thus:

$$\mathcal{E}_z = \frac{ic}{\omega\epsilon}\left[\frac{\partial \mathcal{H}_y}{\partial x} - \frac{\partial \mathcal{H}_x}{\partial y}\right] \tag{7}$$

and

$$\frac{\partial \mathcal{E}_x}{\partial z} = \frac{\partial \mathcal{E}_z}{\partial x} + \frac{i\omega}{c}\mathcal{H}_y \tag{8}$$

where ϵ is the (spatially varying) dielectric constant and c is the velocity of light, and where

$$\begin{aligned}\mathcal{E}_x &= (E_x + E_{xd}e^{iq_x x})e^{i(k_x x + k_y y - \omega t)}, \\ \mathcal{H}_y &= (H_y + H_{yd}e^{iq_x x})e^{i(k_x x + k_y y - \omega t)},\end{aligned} \tag{9}$$

etc. Equations (7) and (8) may be combined in the following form, in which $\mathcal{E}_z$ is eliminated and only elements that are in Ψ appear:

$$\begin{aligned}\frac{\partial \mathcal{E}_x}{\partial_z} &= \frac{ic}{\omega}\left[\left[\frac{\partial}{\partial x}\frac{1}{\epsilon}\right]\left[\frac{\partial \mathcal{H}_y}{\partial x} - \frac{\partial \mathcal{H}_x}{\partial y}\right] + \frac{1}{\epsilon}\frac{\partial}{\partial x}\left[\frac{\partial \mathcal{H}_y}{\partial x} - \frac{\partial \mathcal{H}_x}{\partial y}\right] + \frac{\omega^2}{c^2}\mathcal{H}_y\right] \\ &= \frac{i\omega}{c}\left[\left\{1 + \frac{c^2}{\omega^2}\left[\left[\frac{\partial}{\partial x}\frac{1}{\epsilon}\right]\frac{\partial}{\partial x} + \frac{1}{\epsilon}\frac{\partial^2}{\partial x^2}\right]\right\}\mathcal{H}_y + \frac{c^2}{\omega^2}\left[\left[\frac{\partial}{\partial x}\frac{1}{\epsilon}\right]\frac{\partial}{\partial y} + \frac{1}{\epsilon}\frac{\partial^2}{\partial x\,\partial y}\right](-\mathcal{H}_x)\right].\end{aligned} \tag{10}$$

Three more somewhat simpler second-order partial-differential equations for the electromagnetic field components in Ψ, that is, the components in the (xy) plane, may be obtained in a similar way. They are

$$\frac{\partial \mathcal{H}_y}{\partial z} = \frac{i\omega}{c}\left[\left[\epsilon + \frac{c^2}{\omega^2}\frac{\partial^2}{\partial y^2}\right]\mathcal{E}_x - \frac{c^2}{\omega^2}\frac{\partial^2}{\partial x\,\partial y}\mathcal{E}_y\right], \tag{11}$$

$$\begin{aligned}\frac{\partial \mathcal{E}_y}{\partial z} = \frac{i\omega}{c}&\left[\frac{1}{\epsilon}\frac{c^2}{\omega^2}\frac{\partial^2}{\partial x\,\partial y}\mathcal{H}_y\right. \\ &\left. + \left[1 + \frac{1}{\epsilon}\frac{c^2}{\omega^2}\frac{\partial^2}{\partial y^2}\right](-\mathcal{H}_x)\right],\end{aligned} \tag{12}$$

and

$$-\frac{\partial \mathcal{H}_x}{\partial z} = \frac{i\omega}{c}\left[-\frac{c^2}{\omega^2}\frac{\partial^2}{\partial x\,\partial y}\mathcal{E}_x + \left[\epsilon + \frac{c^2}{\omega^2}\frac{\partial^2}{\partial x^2}\right]\mathcal{E}_y\right]. \tag{13}$$

V. SPATIALLY PERIODIC DIELECTRIC CONSTANT

Next we shall simplify these equations for the special case where, at least for an infinitesimal distance in the z direction,

$$\begin{aligned}\epsilon(z) &= (1+u)[1 + v_c\cos(q_x x) + v_s\sin(q_x x)] \\ &= (1+u)(1 + \alpha e^{iq_x x} + \beta e^{-iq_x x}).\end{aligned} \tag{14}$$

Note that in absorbing media, u, v_c, and v_s may all be complex numbers, with the imaginary parts describing the absorption. Although u, v_c, and v_s may depend on z, we shall suppose that q_x is invariant. Periodic z dependence is discussed in Sec. VI. The terms v_c and v_s are proportional to the complex structure-factor components for a set of Bragg planes that are oblique with respect to the wafer surface, and that are close to the angle for Bragg diffraction of the incident beam. If $\delta = 1 - n$ is the average complex refractive index decrement at this level in the wafer, then $u \approx -2\delta$.

Upon inserting the exponential form of Eq. (14) into Eqs. (10)–(13), the factor $e^{iq_x x}$ appears with some of the Ψ_0 terms of Eq. (4), and the factor $e^{-iq_x x}$ appears with some of the Ψ_d terms of Eq. (5). These terms account for transfer of energy from the undiffracted beams to the diffracted beams and back. There are also Ψ_0 terms with the factor $e^{-iq_x x}$, and Ψ_d terms with the factor $e^{iq_x x}$, in addition to $e^{\pm 2iq_x x}$ and higher Fourier components with both. The effect of these terms is entirely negligible for nearly all x-ray diffraction problems. This is because only diffraction close to a particular Bragg reflection direction characterized by momentum change q_x ever achieves appreciable amplitude. The field components with the factor $e^{iq_x x}$ and those without are orthogonal. Thus there are eight equations among the eight elements of Ψ from Eqs. (10)–(13), which may be written in the matrix form

$$\frac{\partial \Psi}{\partial z} = \frac{i\omega}{c}\underline{D}\Psi. \tag{15}$$

$\underline{D}$ is an 8×8 differential transfer matrix that defines the change in the field Ψ over an infinitesimal displacement in the z direction. The elements of $\underline{D}$ may be found by expanding Eqs. (10)–(13) for Ψ_0 and for Ψ_d with Eq. (14). For compactness, we define $\kappa_x = k_x c/\omega$, where k_x is the x component of the x-ray propagation vector in free space. Note that $\kappa_x = \sin\theta\cos\phi$. Similar substitutions are made for other components of k. We also define $\kappa_x' = \kappa_x + q_x c/\omega$.

We shall break the 8×8 matrix $\underline{D}$ into four quadrants,

$$\underline{D} = \begin{bmatrix}\underline{D}_{00} & \underline{D}_{0d} \\ \underline{D}_{d0} & \underline{D}_{dd}\end{bmatrix}, \tag{16}$$

where subscript d refers to obliquely diffracted beams and 0 to specular or undiffracted beams.

To first order in α and β, the upper left-handed quadrant of $\underline{D}$ is

$$\underline{D}_{00} = \begin{bmatrix} 0 & 1-\kappa_x^2/(1+u) & 0 & \kappa_x\kappa_y/(1+u) \\ 1+u-\kappa_y^2 & 0 & -\kappa_x\kappa_y & 0 \\ 0 & \kappa_x\kappa_y/(1+u) & 0 & 1-\kappa_y^2/(1+u) \\ -\kappa_x\kappa_y & 0 & 1+u-\kappa_x^2 & 0 \end{bmatrix}. \tag{16a}$$

The lower left-hand quadrant, which accounts for transfer of energy from the incident and specularly reflected rays to the diffracted rays, is

$$\underline{D}_{d0}=\alpha e^{iq_x x}\begin{bmatrix} 0 & \kappa'_x\kappa_x/(1+u) & 0 & \kappa'_x\kappa_y/(1+u) \\ 1+u & 0 & 0 & 0 \\ 0 & \kappa_x\kappa_y/(1+u) & 0 & \kappa_y^2/(1+u) \\ 0 & 0 & 1+u & 0 \end{bmatrix} . \tag{16b}$$

The upper right-hand quadrant, which accounts for transfer of energy back from the obliquely diffracted rays to the incident and specular rays, is

$$\underline{D}_{0d}=\beta e^{-iq_x x}\begin{bmatrix} 0 & \kappa'_x\kappa_x/(1+u) & 0 & \kappa_x\kappa_y/(1+u) \\ 1+u & 0 & 0 & 0 \\ 0 & \kappa'_x\kappa_y/(1+u) & 0 & \kappa_y^2/(1+u) \\ 0 & 0 & 1+u & 0 \end{bmatrix} . \tag{16c}$$

The lower right-hand quadrant, which has the same effect on the diffracted beams as the upper left-hand quadrant has on the undiffracted beams, is

$$\underline{D}_{dd}=\begin{bmatrix} 0 & 1-\kappa'^2_x/(1+u) & 0 & \kappa'_x\kappa_y/(1+u) \\ 1+u-\kappa_y^2 & 0 & -\kappa'_x\kappa_y & 0 \\ 0 & \kappa'_x\kappa_y/(1+u) & 0 & 1-\kappa_y^2/(1+u) \\ -\kappa'_x\kappa_y & 0 & 1+u-\kappa'^2_x & 0 \end{bmatrix} . \tag{16d}$$

To integrate Eq. (15), think of the crystal wafer as a series of thin, parallel layers, through each of which the terms in ϵ [Eq. (14)] are practically invariant with z. If this is the case, then the wave function, Ψ_2, at the second surface of the thin layer is related to that at the first, Ψ_1, by the equation

$$\Psi_2=\exp\left[\frac{i\omega}{c}\tau\underline{D}\right]\Psi_1=\underline{P}(\tau)\Psi_1 \tag{17}$$

where τ is the thickness of the thin layer and

$$\exp\left[\frac{i\omega}{c}\tau\underline{D}\right]=1+\frac{i\omega}{c}\tau\underline{D}+\left[\frac{i\omega}{c}\right]^2\frac{\tau^2}{2!}\underline{D}\,\underline{D}+\cdots . \tag{18}$$

The latter series is continued until the factor before the $\underline{D}$'s is on the order of 10^{-8}. The transfer matrix between the top of a wafer of thickness $\mathcal{N}$ and the bottom can always be found from the matrix equation

$$\underline{P}(\mathcal{N})=\underline{P}(\tau_n)\underline{P}(\tau_{n-1})\cdots\underline{P}(\tau_2)\underline{P}(\tau_1) , \tag{19}$$

where $\underline{P}(\tau_j)$ is the transfer matrix for thin layer j.

VI. TWO SETS OF BRAGG PLANES, OBLIQUE AXIS TRANSFORMATION

In principle, Eq. (19) could be used directly to find the transfer matrix for any wafer that can be described as a stack of gratings of equal lattice spacing. The casual reader may wish to skip Secs. VI and VII, which deal with methods of enhancing the speed of computation when there are regions where the layering is also periodic, as in a crystal.

Suppose that at most two sets of Bragg planes are involved in the diffraction of the incident or diffracted beam to a significant extent. In the vicinity of one depth, z, in a crystal, one of these sets will be tilted at an angle σ with respect to the surface and will have a Bragg spacing B_σ. The grating spacing, $g=B_\sigma/\sin\sigma$, is independent of depth, as shown in Fig. 2. The only other set of Bragg planes that will be considered here are those parallel to the surface, with variable Bragg spacing B_p. Then the dielectric constant near this depth can be represented by

$$\begin{aligned}\epsilon&=[1+u_b+u_c\cos(pz)+u_s\sin(pz)](1+\alpha e^{i(q_x x+q_z z)}+\beta e^{-i(q_x x+q_z z)}) \\ &=[1+u_b+u_c\cos(pz)+u_s\sin(pz)][1+v_c\cos(q_x x+q_z z)+v_s\sin(q_x x+q_z z)] ,\end{aligned} \tag{20}$$

where $p=2\pi/B_p$ and $q_z=2\pi(\cos\sigma)/B_\sigma=q_x\cot\sigma$ [cf. Eq. (14)]. Note that, in general, all of the parameters in Eq. (20) except q_x may vary with z, but they do not vary within an unstrained crystal.

The oblique Bragg planes have a periodicity $\mathcal{N}(z)=B_\sigma(z)/\cos[\sigma(z)]$ along the z axis that is not necessarily rationally related to the periodicity $B_p(z)$ of the planes parallel to the surface, as shown in Fig. 2. If diffraction of one incident beam by both sets of planes is appreciable, it is convenient to change from the x coordinate to a coordinate ξ measured from an oblique, possibly curved line that intersects the intersections of the two sets of Bragg planes diagonally as shown in Fig. 2. This curved line is defined by the equation $x-\xi=\eta(z)$, where

$$\eta(z)=\int_0^z\left[\frac{p(z)}{q_x}-\frac{q_z(z)}{q_x}\right]dz=\int_0^z\left[\frac{g}{B_p(z)}-\frac{g}{\Lambda(z)}\right]dz\ . \tag{21}$$

Through this transformation Eq. (20) becomes

$$\epsilon=[1+u_b+u_c\cos(pz)+u_s\sin(pz)]\times(1+\alpha e^{i(q_x\xi+pz)}+\beta e^{-i(q_x\xi+pz)})\ , \tag{20'}$$

so that a full cycle across both sets of planes occurs at the same value of z along the path $x=\eta(z)$. A realistic model of surface strain in many cases is one in which B_p and Λ change by the same small factor, corresponding to a small expansion or contraction in the z direction only.

Let us define $\underline{P}_\eta(\tau)$ over short vertical intervals τ at points along the path $\eta(z)$ in the same way that $\underline{P}(\tau)$ was defined in terms of $\underline{D}$ along the z axis. Also define a matrix $\underline{R}$ to shift horizontally, parallel to the surfaces. Then the "integration" defined by Eq. (19) can be replaced by an equivalent stair-step contour along the line $x=\eta(z)$, followed by a single transfer back to the z axis, as shown in Fig. 4. The matrix $\underline{R}(x_2-x_1)$ is diagonal with elements

$$R_{11},\ldots,R_{44}=e^{ik_x(x_2-x_1)}$$

and (22)

$$R_{55},\ldots,R_{88}=e^{i(k_x+q_x)(x_2-x_1)}\ .$$

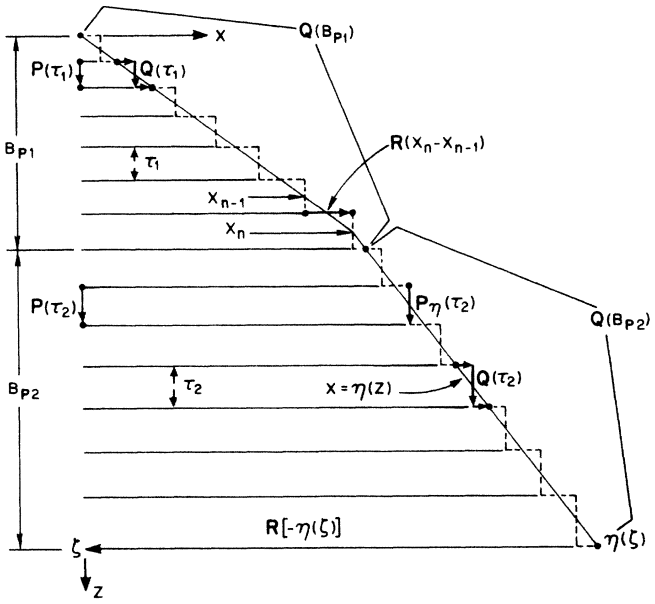

FIG. 4. Two paths of "integration" to obtain the total transfer matrix $\underline{P}(\zeta)$; one straight down and the other in a stair-step along the cell diagonal, $\eta(z)$, followed by a transfer back to $x=0$. Vertical transfers away from the origin are designated $\underline{Q}$, and horizontal ones $\underline{R}$. Only two cycles, one of thickness B_{p1} and one of thickness B_{p2}, are represented, each divided into seven subintervals of thickness τ_1 or τ_2.

For a straight section of the path $\eta(z)$, the stair-step contour may be made up of a series of elements,

$$\underline{Q}(\tau)=\underline{R}\left[\frac{\tau}{2}\frac{\partial\eta}{\partial z}\right]\underline{P}_\eta(\tau)\underline{R}\left[\frac{\tau}{2}\frac{\partial\eta}{\partial z}\right]\ . \tag{23}$$

Equations (22) and (23) allow us to treat an oblique set of Bragg planes and a set parallel to the surface as if they had the same periodicity normal to the surfaces, using Eq. (24) in the next section.

VII. FAST COMPUTATION FOR PERIODIC REGIONS

Even in distorted crystals the wafer will ordinarily be divisible into sublayers that are almost exactly periodic over many cycles. If a wafer of thickness ζ can be represented to good approximation by m cycles of thickness Λ_1, followed by n cycles of a different thickness Λ_2, then much computer time can be saved by using

$$\underline{P}(\zeta)=\underline{R}(-\eta(\zeta))\underline{Q}(\Lambda_2)^n\underline{Q}(\Lambda_1)^m\ . \tag{24}$$

If planes parallel to the surface are not important, the cycle thickness is set to $\Lambda(z)=B_\sigma(z)/\cos[\sigma(z)]$, $\underline{R}$ is unity, and $\underline{Q}$ is replaced by $\underline{P}$ in Eq. (24). As explained in other papers on matrix optics of periodic media, a high power of a matrix may be obtained quickly by repeatedly squaring the matrix for one cycle, and multiplying the accumulated product by the latest square if the corresponding digit in the binary representation of the high power is unity, or not doing so if it is zero.

If neither the incident nor the diffracted beam is near the Bragg angle for planes parallel to the surface, then the cycle length Λ may be chosen arbitrarily. The exponential series (18) converges rapidly and accurately so long as $\tau\omega/c$ is less than unity. The computation for a thick layer goes fastest using a moderately short interval such as $\tau\omega/c\approx 1/8$.

If the Bragg planes parallel to the surface are important, the appropriate cycle length is the Bragg spacing B_p. The transfer matrix for one cycle, $\underline{P}(B_p)$ or $\underline{Q}(B_p)$, can be computed with considerable accuracy using only four equal subintervals, with an average value of ϵ in each subinterval, and using Eq. (19) or its $\underline{Q}$ equivalent over one cycle. (Figure 4 is drawn with seven subintervals per cycle.)

VIII. MATCHING BOUNDARY FIELDS

If the whole wafer is uniformly periodic, as in an unstrained crystal, a normal-mode analysis of the matrix for a single cycle, $\underline{Q}(\Lambda)$ or $\underline{P}(\Lambda)$, can give insight into the propagating modes.[7] This procedure becomes tedious in a strained crystal and is unnecessary when the object of the computation is to evaluate Ψ at one or more particular levels, given the incident-beam direction and polarization. Instead we generate the matrix $\underline{P}$ for the whole wafer and solve the boundary-matching equations for reflected, reflected-diffracted, transmitted, and transmitted-diffracted beams.

If there is reason to want to examine the electromagnetic field components at some level z between the surfaces of the crystal wafer, it can be done after solving the

boundary-value problem by saving the matrix $\underline{P}(z)$ as the full matrix $\underline{P}(\zeta)$ is being computed, or by reevaluating $\underline{P}(z)$, and then multiplying the field $\Psi(0)$ by that matrix.

In cases where the transmitted beam is extremely weak, because of either absorption or extinction, the matrix $\underline{Q}$ or $\underline{P}$ has some extremely large elements and the method may begin to lose accuracy because of numerical truncation errors. We monitor $Q_{11}Q_{22}+Q_{12}Q_{21}$ and $Q_{55}Q_{66}+Q_{56}Q_{65}$, which are the combinations of elements that grow largest in such situations. If the sum of the absolute values of these combinations exceeds about 10^8, we halt the matrix multiplications in Eq. (24). (We are doing computations with about 16-octal-digit precision. With more precision this factor could be increased.) This truncation has negligible effect on the computed wave function in any region where it is of appreciable amplitude.

The energy flux normal to the wafer surface can be found by evaluating Poynting's vector in the upward- or downward-wave contributions to the wave functions Ψ. Two orthogonal basis vectors for the incident wave functions at the first surface in vacuum, the s- and p-polarized waves, are

$$\psi_{is}=\frac{1}{(\kappa_z)^{1/2}}\begin{bmatrix}\sin\phi\\-\kappa_z\sin\phi\\-\cos\phi\\\kappa_z\cos\phi\\0\\0\\0\\0\end{bmatrix}$$

and (25)

$$\psi_{ip}=\frac{1}{(\kappa_z)^{1/2}}\begin{bmatrix}-\kappa_z\cos\phi\\\cos\phi\\-\kappa_z\sin\phi\\\sin\phi\\0\\0\\0\\0\end{bmatrix},$$

where

$$\kappa_z=k_zc/\omega=(1-\kappa_x^2-\kappa_y^2)^{1/2}=\cos\theta\ .$$

This and subsequent basis vectors are normalized to give the same constant value of the z component of Poynting's vector or $E_xH_y-E_yH_x$. The two corresponding basis vectors for waves reflected from Bragg planes parallel to the surfaces or specularly reflected are

$$\psi_{rs}=\frac{1}{(\kappa_z)^{1/2}}\begin{bmatrix}-\sin\phi\\-\kappa_z\sin\phi\\\cos\phi\\\kappa_z\cos\phi\\0\\0\\0\\0\end{bmatrix}$$

and (26)

$$\psi_{rp}=\frac{1}{(\kappa_z)^{1/2}}\begin{bmatrix}\cos\phi\\\kappa_z\cos\phi\\\sin\phi\\\kappa_z\sin\phi\\0\\0\\0\\0\end{bmatrix}.$$

The two undiffracted transmitted unit vectors are

$$\psi_{ts}=\frac{1}{(\kappa_z')^{1/2}}\begin{bmatrix}\sin\phi\\-\kappa_z'\sin\phi\\-\cos\phi\\\kappa_z'\cos\phi\\0\\0\\0\\0\end{bmatrix}$$

and (27)

$$\psi_{tp}=\left[\frac{\epsilon_s}{\kappa_z'}\right]^{1/2}\begin{bmatrix}-(\kappa_z'/\epsilon_s)\cos\phi\\\cos\phi\\-(\kappa_z'/\epsilon_s)\sin\phi\\\sin\phi\\0\\0\\0\\0\end{bmatrix},$$

where

$$\kappa_z'=k_z'c/\omega=(\epsilon_s-\kappa_x^2-\kappa_y^2)^{1/2}$$

is the vertical component of κ in the substrate, for which the dielectric constant, which may be complex, is ϵ_s.

The upward-diffracted waves are

$$\psi_{rsd}=\frac{1}{(\kappa_{zd})^{1/2}}\begin{bmatrix}0\\0\\0\\0\\-\sin\phi_d\\-\kappa_{zd}\sin\phi_d\\\cos\phi_d\\\kappa_{zd}\cos\phi_d\end{bmatrix}$$

and (28)

$$\psi_{rpd}=\frac{1}{(\kappa_{zd})^{1/2}}\begin{bmatrix}0\\0\\0\\0\\\kappa_{zd}\cos\phi_d\\\cos\phi_d\\\kappa_{zd}\sin\phi_d\\\sin\phi_d\end{bmatrix}e^{ik_{zd}z},$$

where

$$\kappa_{zd}=k_{zd}c/\omega=(1-\kappa_x'^2-\kappa_y^2)^{1/2}=\cos\theta_d$$

and ϕ_d is the azimuth of the diffracted beam. Finally, the downward-diffracted waves are

$$\psi_{tsd}=\frac{1}{(\kappa_{zd}')^{1/2}}\begin{bmatrix}0\\0\\0\\0\\\sin\phi_d\\-\kappa_{zd}'\sin\phi_d\\-\cos\phi_d\\\kappa_{zd}'\cos\phi_d\end{bmatrix}$$

and (29)

$$\psi_{tpd}=\left[\frac{\epsilon_s}{\kappa_{zd}'}\right]^{1/2}\begin{bmatrix}0\\0\\0\\0\\-(\kappa_{zd}'/\epsilon_s)\cos\phi_d\\\cos\phi_d\\-(\kappa_{zd}'/\epsilon_s)\sin\phi_d\\\sin\phi_d\end{bmatrix},$$

where $\kappa_{zd}'=k_{zd}'c/\omega=(\epsilon_s-\kappa_x'^2-\kappa_y^2)^{1/2}$.

In order to find the reflected, transmitted, and upward- and downward-diffracted wave functions from an incident s-polarized wave, the set of eight simultaneous equations

$$\rho_{ts}^s\psi_{ts}+\rho_{tp}^s\psi_{tp}+\rho_{tsd}^s\psi_{tsd}+\rho_{tpd}^s\psi_{tpd}\equiv\Psi_s(\zeta)=\underline{P}(\zeta)(\psi_{is}+\rho_{rs}^s\psi_{rs}+\rho_{rp}^s\psi_{rp}+\rho_{rsd}^s\psi_{rsd}+\rho_{rpd}^s\psi_{rpd})\equiv\underline{P}(\zeta)\Psi_s(0) \quad (30)$$

are solved for the eight complex amplitude coefficients ρ^s. A similar set of equations, wherein the vector sum at the first surface starts with $\psi_{ip}+\rho_{rs}^p\psi_{rs}+\cdots$, gives the amplitudes ρ^p of the corresponding waves when the incident wave is p polarized.

As suggested previously, once $\Psi(0)$ has been evaluated, the electromagnetic field at any level z can be determined by obtaining the transfer matrix between the first surface and the surface at that level, and solving the equation $\Psi(z)=\underline{P}(z)\Psi(0)$.

IX. DISPERSION, STRUCTURE FACTORS, AND AMPLITUDES IN ϵ

The classical nonrelativistic dispersion formula for a local dielectric constant in Gaussian units (see Ref. 11, Eq. (4.35) is

$$\epsilon=1+\sum_j\left[\frac{4\pi\rho_j}{(k_j^2-k^2)/r_e+2ik^3/3}\right], \quad (31)$$

where $\hbar ck$ is the incident-x-ray photon energy, ρ_j is the local number of electrons per unit volume having binding energy $\hbar ck_j$, and r_e is the classical electron radius, with q_e^2/m_ec^2 in Gaussian units. The coefficients v and u can be determined from the Fourier expression

$$\begin{Bmatrix}v_c\\v_s\end{Bmatrix}\text{ or }\begin{Bmatrix}u_c\\u_s\end{Bmatrix}=\frac{1}{V}\int_0^a\int_0^b\int_0^c\epsilon\times\begin{Bmatrix}\cos\\\sin\end{Bmatrix}[2\pi(hx+ky+lz)]\times dx\,dy\,dz\ , \quad (32)$$

where V is the unit-cell volume, x,y,z are the unit-cell coordinates, a,b,c are the unit-cell dimensions, and h,k,l may be the Miller indices of either the oblique or the parallel Bragg planes.

Although good models of electronic shell densities are available, it may be easier to obtain equivalent information using tables of atomic structure factors with dispersion corrections,[12]

$$f=f_0[(\sin\theta_B/\lambda]+\Delta f'(\lambda)+i\Delta f''(\lambda)\ ,$$

where $\lambda=2\pi/k$ is the x-ray wavelength and θ_B is the Bragg angle. If $k\gg k_j$ for all j, then $f\approx f_0$.

The amplitudes of the sinusoidally varying parameters in ϵ can be written as

$$\begin{Bmatrix} v_c \\ v_s \end{Bmatrix} \text{ or } \begin{Bmatrix} u_c \\ u_s \end{Bmatrix} = G \sum_i e^{-M_i} f_i \begin{Bmatrix} \cos \\ \sin \end{Bmatrix} [2\pi(hx_i + ky_i + lz_i)] , \quad (33)$$

where x_i, y_i, z_i is the mean location of the nucleus of atom i and e^{-M_i} is a Debye-Waller factor to take account of the thermal motion of that atom (see Ref. 11, Eq. 6.100). The numerical factor

$$G = \frac{-4\pi r_e}{k^2 V} , \quad (34)$$

where V is the unit-cell volume, relates structure factors to variations of dielectric constant. (See Ref. 11, Eq. 4.46, and recall that $\epsilon - 1 \approx -2\delta$.) To understand the physical significance of G, compare Eqs. (31)–(33) and note that the structure factor f_i is a sort of modified count of electrons whose maximum value is the atomic number of the atom. Then the sum of f_i/V is a modified total electron density, ρ, within the unit cell.

X. NUMERICAL EXAMPLES

We shall use the example mentioned in the Introduction, InP cut parallel to the (111) planes with diffraction from the (200) planes, in the following illustrations. We shall also suppose that the incident radiation is the Cu $K\alpha_1$ line with wavelength 1.5405 Å, and shall ignore its spectral linewidth. The nominal Bragg angle for the (111) planes is 13.1384° and that for the (200) planes is 14.9557°. The diffraction cones for these two sets of planes are illustrated in Fig. 5. The direction of the edges of the tilted (200) planes at the edge of the wafer is also illustrated. In each example, the tilt of the (200) planes is in such a direction with respect to the incident beam that q_x is a negative quantity.

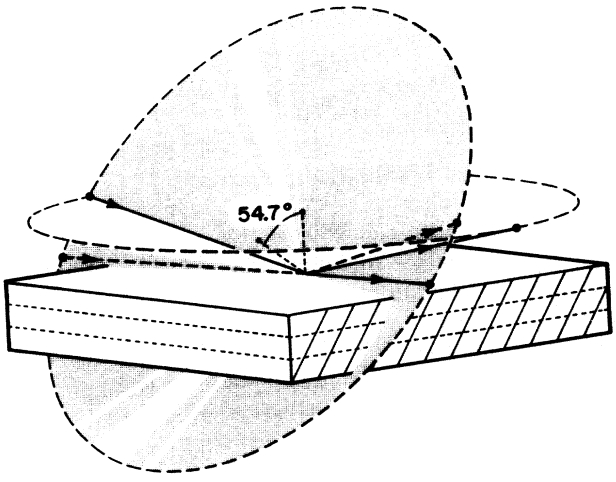

FIG. 5. Computer-aided perspective sketch of diffraction cones for the tilted (200) planes and the (111) planes parallel to the surface. Dashed beam at grazing incidence gives spectrum in Fig. 6. Solid beam incident on cone intersection is diffracted onto both cones, and residual transmittance is shown in Fig. 8.

The cones are not infinitely thin, but represent narrow envelopes over which appreciable radiation of this wavelength will be diffracted. All spectral bands will be computed for fixed incident azimuth and will be expressed over a range of polar angles, θ, of the incident beam. It should be remembered, however, that if the incident wavelength, azimuth and polar angle are all fixed, then the directions of the (200) and the (111) diffraction are also fixed. If any one of the incident parameters is allowed to vary, then the diffracted beam parameters will vary in accordance with the grating equations (2) and (3). Thus both θ and ϕ of the incident beam could have been fixed and the wavelength varied. Only results for σ-polarized radiation (E field parallel to the crystal surface) are shown. The results for π-polarized radiation are not very different in any of the cases considered because the Bragg angle is far from 45°. Optical parameters assumed in the computations [cf. Eqs. (14) and (20)] are

$$u_b = (-2.702 + i0.2953) \times 10^{-5} ,$$

$$u_c = (-3.590 + i0.4555) \times 10^{-5} ,$$

and

$$u_s = (-1.010 + i0.1350) \times 10^{-5}$$

for the (111) planes parallel to the surface, and

$$v_c = (-2.517 + i0.3205) \times 10^{-5}$$

and $v_s = 0$ for the tilted (200) planes. The phases are based on placement of the origin at an indium atom on the surface, ignoring possible displacement from the regular lattice.

Our first example is to show how diffraction from oblique planes is affected when the incident beam is near grazing incidence. Suppose the incident radiation is at a fixed azimuth $\phi = 72°$. Then the peak of the beam that is Bragg diffracted from the (200) planes will be incident at a polar angle of 88.87°, as shown on the left in Fig. 6. The penetration of the beam will be relatively small because the incident beam is the near-grazing incidence for Bragg diffraction, and because of the large absorption by InP at this wavelength. Consequently, the diffracted band will be relatively broad, with radiation at different angles of incidence being diffracted in different directions determined uniquely by the equations for optical diffraction gratings, assuming that the area of the crystal surface is large. Diffraction bands for three slightly smaller azimuths of incidence are also shown. These azimuths are such that the polar angles for the Bragg peaks are even nearer to grazing incidence. The beam penetration is even less and the diffraction band becomes weaker and broader.

The dashed line in Fig. 6 shows the adjacent onset of specular "total external reflection." This curve is invariant as long as the diffraction band is outside it. The diffraction band for incident azimuth $\phi = 71.25°$, for which the polar angle of incidence for peak intensity is about $\theta = 89.7°$, distorts the "total reflection" curve so

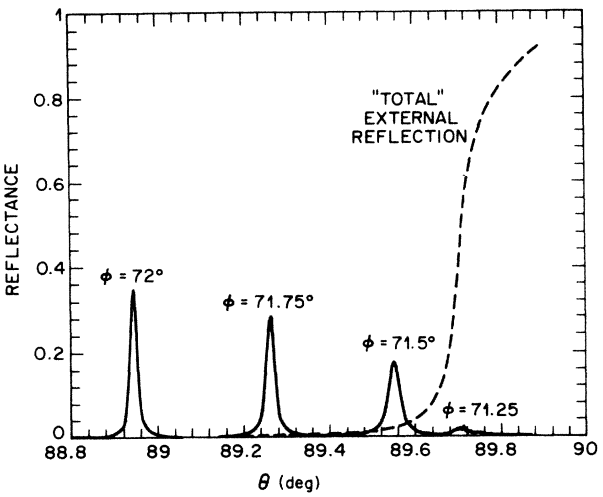

FIG. 6. Diffracted intensity relative to incident intensity vs polar angle of incidence, θ, near grazing incidence (dashed beams in Fig. 5), computed for Cu $K\alpha_1$ x rays diffracted from the (200) planes of a thick InP wafer cut parallel to the (111) planes. Solid curves are for various azimuthal angles, ϕ. Dashed curve shows the onset of "total external reflection." All results are for σ-polarized incident radiation.

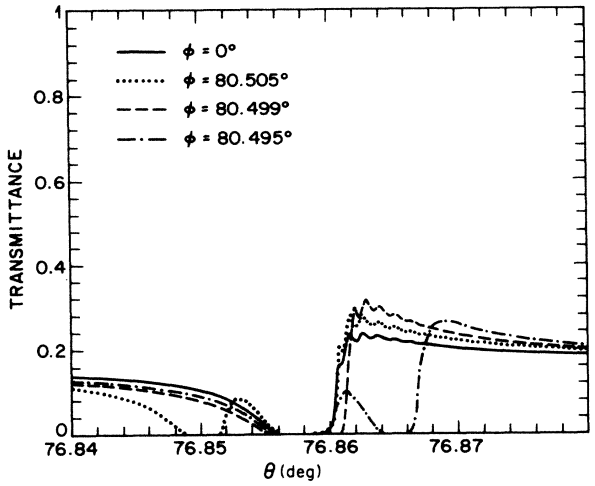

FIG. 8. Transmission by an InP wafer 33 886 Å [10 000 (111) layers] thick. Dotted and dashed curves are for azimuth near conjunction of asymmetric Laue diffraction by (200) planes and symmetric Bragg diffraction by (111) planes (solid beams in Fig. 5). Solid curve is for azimuth far from this conjunction. Dip due to (200) reflection moves from polar angle $\theta = 76.85°$ at azimuth $\phi = 80.505°$ through the (111) band to $\theta = 76.865°$ at $\phi = 80.495°$.

slightly that we do not show the distortion. The roughness of the low, broad diffraction peak for the last case is caused by numerical roundoff error associated with the extremely small intensity of the transmitted beam.

Spectral broadening of the diffraction peak at fixed angle or, in the cases to follow, angular broadening at fixed wavelength, may also be achieved by causing the crystal layers near the surface to curve or to have a different spacing, by using ion implantation, by growing an epitaxial layer of varying stoichiometry, or by other means. As an example, we show the relative diffraction intensity for the case where the incident and diffracted beams are about equally high above the crystal surface. We suppose that the crystal wafer is thick but that the upper thousand planes have been expanded slightly in the z direction, so that Λ and the (111) spacing, B_p, are 1.001 times as large as in the underlying material. The results are shown in Fig. 7. The dashed curve is the oblique Darwin band for the unstrained substrate alone. Not only two bands characteristic of the two slightly different Bragg spacings appear in the spectrum for the distorted crystal, but small subsidiary peaks also appear on either side. Such extra features are very sensitive to details of the model of the strain distribution, and are very useful in determination of structure near the surface.[13]

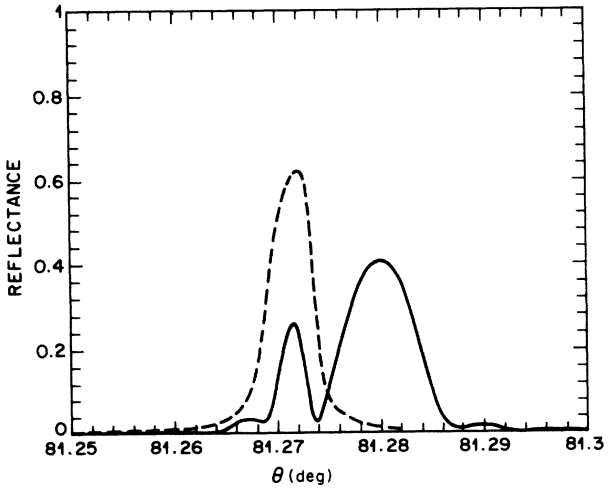

FIG. 7. Bragg diffraction spectrum as in Fig. 6, but far from grazing incidence; $\theta' \approx 180° - \theta$. Dashed line: spectrum from uniform unstrained thick wafer. Solid line: diffraction by InP with upper 3389 Å [1000 (111) layers] expanded by a factor of 1.001 in the z direction.

Interference effects near the intersection of the (111) and the (200) diffraction cones, or Kossel lines, are illustrated in Fig. 8. In this case, we consider transmission through a wafer only 10000 times the (111) spacing in thickness. The solid curve there is the transmission when the azimuth is zero, so that the effect of the (200) planes is remote and the depression in transmission is due solely to the (111) diffraction. In the present examples, beams diffracted by the (200) planes go into the wafer (Laue case), while those from the (111) planes reemerge from the upper side (Bragg case). The transmitted beams are attenuated by Bragg diffraction from either set of diffracting planes. The structure is complicated by the interference effects around the intersection of the two diffraction bands. An additional complication comes from Pendellösung fringes, since the wafer has finite

thickness and the angle of incidence is variable. We were interested to note that the Borrmann anomalous transmission effect,[14] which is the rise on the right-hand side of each transmission minimum, is enhanced considerably, particularly when the (111) and the (200) peaks coincide at $\phi \approx 80.499°$. Most of these features would require special procedures to simulate without the 8×8 matrix method.

---

[1]See, for example, R. W. James, *The Optical Principles of the Diffraction of X-Rays* (Bell, London, 1958), Chap. 8.
[2]A. M. Afanas'ev and M. K. Melkonyan, Acta. Crystallogr. Sect. A **39**, 207 (1983).
[3]S. Takagi, J. Phys. Soc. Jpn. **26**, 1239 (1969).
[4]D. Taupin, Bull. Soc. Fr. Mineral Cristallogr. **87**, 469 (1964).
[5]J. Billard, Thesis, University of Paris (1966).
[6]S. Teitler and B. Henvis, J. Opt. Soc. Am. **60**, 830 (1970).
[7]D. W. Berreman, J. Opt. Soc. Am. **62**, 502 (1972).
[8]F. Abelès, Ann. Phys. (Paris) **5**, 596 (1950).
[9]K. Rokushima and J. Yamakito, J. Opt. Soc. Am. **73**, 901 (1983).
[10]D. W. Berreman, Opt. Eng. **25**, 933 (1986).
[11]A. H. Compton and S. K. Allison, *X-Rays in Theory and Experiment*, 2nd ed. (Van Nostrand, New York, 1935), pp. 277, 280, and 438.
[12]*International Tables for X-Ray Crystallography*, edited by J. A. Ibers and W. C. Hamilton (Kynoch, Birmingham, England, 1974). See Vol. IV, p. 148 for explanation.
[13]Similar work, limited to symmetrical Bragg diffraction, appears in A. T. Macrander, E. R. Minami, and D. W. Berreman, J. Appl. Phys. **60**, 1364 (1986).
[14]G. Borrmann, Phys. Z **42**, 157 (1941).

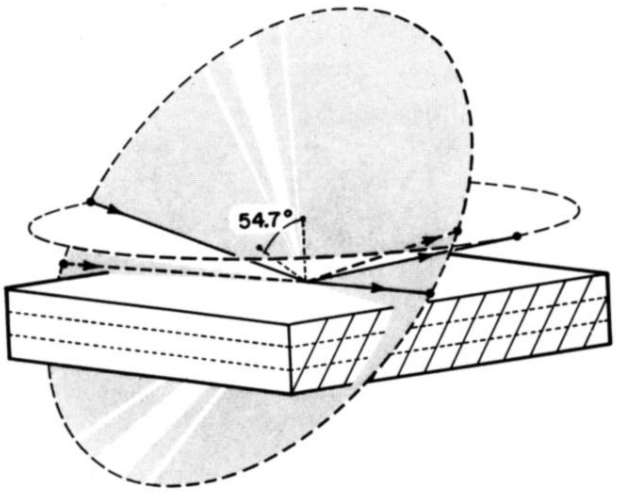

FIG. 5. Computer-aided perspective sketch of diffraction cones for the tilted (200) planes and the (111) planes parallel to the surface. Dashed beam at grazing incidence gives spectrum in Fig. 6. Solid beam incident on cone intersection is diffracted onto both cones, and residual transmittance is shown in Fig. 8.